Activity-induced gene expression in the human brain

Snehajyoti Chatterjee[1,2#], Brian J. Park[3#], Yann Vanrobaeys[1#], Shane A. Heiney[1,2,4], Ariane E. Rhone[3], Kirill V. Nourski[3], Lucy Langmack[1,2], Utsav Mukherjee[1,2], Christopher K. Kovach[3], Zsuzsanna Kocsis[3,5], Yukiko Kikuchi[5], Christopher I. Petkov[3,5], Marco M. Hefti[6], Ethan Bahl[7], Jacob J Michaelson[7], Hiroto Kawasaki[3], Hiroyuki Oya[3], Matthew A. Howard III[3], Thomas Nickl-Jockschat[1,2,7], Li-Chun Lin[1,2,8], Ted Abel[1,2,7*]

Affiliations:

[1] Department of Neuroscience and Pharmacology, Iowa Neuroscience Institute Carver College of Medicine, University of Iowa, Iowa City, IA, USA

[2] Iowa Neuroscience Institute, University of Iowa, Iowa City, IA, USA

[3] Department of Neurosurgery, University of Iowa Hospitals and Clinics, Iowa City, IA, USA

[4] Neural Circuits and Behavior Core, Iowa Neuroscience Institute Carver College of Medicine, University of Iowa, Iowa City, IA, USA

[5] Biosciences Institute, Newcastle University Medical School, Newcastle upon Tyne, UK

[6] Department of Pathology, University of Iowa Hospitals and Clinics, Iowa City, IA, USA

[7]Department of Psychiatry, University of Iowa Hospitals and Clinics, Iowa City, IA, USA

[8]Iowa NeuroBank Core, Iowa Neuroscience Institute Carver College of Medicine, University of Iowa, Iowa City, IA, USA

[#]Authors contributed equally

*Corresponding author: ted-abel@uiowa.edu

Keywords:

Electrical stimulation, microglia, anterior temporal neocortex, single nuclei multiomics

Key findings

- Electrical stimulation of the human cortex allows the identification of an activity-dependent gene expression signature.
- Neurons and microglia in the human brain exhibit distinct transcriptional signatures following electrical stimulation.
- Single nuclear chromatin accessibility studies reveal cell-type-specific epigenomic changes and specific transcription factor motifs in microglia.

Abstract

Activity-induced gene expression underlies synaptic plasticity and brain function. Here, using molecular sequencing techniques, we define activity-dependent transcriptomic and epigenomic changes at the tissue and single-cell level in the human brain following direct electrical stimulation of the anterior temporal lobe in patients undergoing neurosurgery. Genes related to transcriptional regulation and microglia-specific cytokine activity displayed the greatest induction pattern, revealing a precise molecular signature of neuronal activation in the human brain.

Main

Activity-induced gene expression underlies the ability of the brain to learn and adapt to environmental stimuli. Dynamic changes in transcriptomic patterns are essential for cognition[1-3], affective processing[4], addiction[5], and the initiation of behaviors[6,7]. However, these experiments have been mostly conducted in rodents[8,9] and human induced pluripotent stem cells[10], and it remains unknown how closely they reflect actual processes in the living human brain. Studies of activity-dependent gene expression in humans *in vivo* are lacking due to the availability and accessibility of tissue that can be acutely manipulated. Direct current electrical stimulation is used in the field of epilepsy surgery and could provide a major avenue to address this important challenge. Stimulation of the amygdala in epileptic patients enhances declarative memory[11], and closed-loop stimulation of the lateral temporal cortex rescues intervals of poor memory encoding[12]. Moreover, electrical stimulation is an effective, therapeutic tool to improve memory[12] and depression[13]. Here, we applied direct electrical stimulation of the anterior temporal lobe of patients undergoing neurosurgery to examine activity-dependent changes in gene expression and chromatin accessibility in the human brain for the first time.

We recruited 8 adult neurosurgical patients undergoing surgical resection of seizure foci following clinical monitoring to treat epilepsy. The patients underwent an anterior temporal lobectomy, during which samples were resected from the neocortex and processed immediately after removal. The participants were evenly distributed between two experimental paradigms. For the first group (stimulated paradigm, n=4 subjects), a

sample was at baseline and then an adjacent region of cortex was stimulated using bipolar electrical stimulation (50 Hz). Thirty minutes later, a sample was taken from the stimulated region **(Fig. 1a; Extended Data Fig. 1, Supplementary Table 1)** In the second group (unstimulated paradigm, n=4 subjects), a sample was taken at baseline and then 30 min later a second sample was taken without stimulation **(Fig. 1b; Extended Data Fig. 1)**. Tissue was subjected to whole-transcriptome RNA sequencing (RNA-seq) to identify activity-induced genes following electrical stimulation. RNA-seq analysis from the stimulated and baseline samples revealed 124 significantly differentially expressed genes induced by electrical stimulation, with 112 up-regulated and 12 down-regulated **(Fig. 1c**; FDR<0.05, log2fold change>0.2; **Supplementary Table 2).** Among the up-regulated genes, we observed induced expression of *NPAS4*, *FOS*, and *NR4A1*, as well as cytokine-related genes *CCL3, CCL4, OSM,* and *RGS1.* Notably, these genes were not significantly enriched for previously identified genes induced in regions showing seizure activity in the human brain **(Extended Data Fig. 2)** [14]. Enrichment network analysis was used to identify the pathways most represented among the 124 differentially expressed genes in the stimulation paradigm. The pathways include transcription at RNA polymerase II promoter, positive regulation of DNA-dependent transcription, cytokine activity, chemokine activity, and cytokine receptor binding **(Extended Data Fig. 3)**. Additional protein-protein interaction (PPI) analysis of the stimulated samples revealed two significant clusters enriched with genes involved in DNA-binding transcription activator activity (RNA Pol II) and cytokine activity **(Fig. 1d)**. RNA-seq analysis comparing unstimulated samples with baseline identified differential expression of only 16 genes, with 9 up-regulated and 7 down-regulated

genes; only NR4A3 overlapped between stimulated and unstimulated groups **(Fig. 1e, Supplementary Table 3).** The lack of extensive overlap between the differentially expressed genes observed in our unstimulated and stimulated groups suggests that the selective changes in gene expression that we see following electrical stimulation do not reflect disease state or surgical conditions such as craniotomy, brain temperature, and anesthesia, but reflect stimulation-induced changes. To investigate if these gene expression changes are unique to human samples and to further determine if they are related to disease state[14,15], we used a similar electrical stimulation paradigm in mouse non-primary auditory cortex and observed the upregulation of genes associated with DNA-binding transcription factor activity (*Fos*, *Fosb*, and *Egr2*) and cytokine activity (*Ccl3* and *Ccl4*) (**Extended Data Fig. 4**). Thus, our findings of activity-dependent genes in response to electrical stimulation in the human brain reveal a molecular signature that is conserved across species.

Next, we investigated the cell types exhibiting differential gene expression following electrical stimulation in the human brain by single nuclei multiomics (RNA and ATAC) on samples from the stimulated paradigm (**Fig 2a**). We sequenced 18,342 nuclei and detected 46,849 unique molecular identifiers and 2,133 median genes per nucleus (**Extended Data Fig. 5a**). Cell clustering analysis identified 7 major cell types in our samples (**Fig. 2b, c**). Importantly, the distribution and proportion of cell types was consistent across baseline and stimulated conditions (**Extended Data Fig. 5b**). We identified differentially expressed genes following electrical stimulation for the following cell types—excitatory neurons, microglia, vip-Sncg-Lamp5 inhibitory neurons, pvalb-Sst

inhibitory neurons, oligodendrocytes, oligodendrocytes precursor cells (OPC), and astrocytes (**Fig. 2d-f, Supplementary Table 4**). Microglia displayed the highest differential gene expression of all cell types with 306 up- and 296 down-regulated genes (**Fig. 2d**). Genes related to cytokine activity (*CCL3*, *CCL4*, *IL1B*, *CCL2*, *IL1A*, *OSM* and *RGS1*) were upregulated exclusively within microglia (**Fig. 2e; Extended Data Fig. 6a**). In contrast, genes related to DNA-binding transcription activity (*FOS*, *EGR1*, *JUNB,* and *EGR3*) were upregulated in neurons and microglia, whereas *NPAS4* and *EGR4* were exclusively upregulated within excitatory and inhibitory neurons (**Fig. 2f, Extended Data Fig. 6b**). Gene expression changes from microglia in the single nuclei multiomic experiment significantly correlated with the bulk RNA-seq (**Fig. 2g, Extended Data Fig. 7-9)**. Interestingly, among the upregulated genes identified in bulk RNA-seq, we discovered that 37 were upregulated in microglia. These results reveal that electrical stimulation activates gene expression involved in transcriptional regulation in multiple cell types and selectively activates genes involved in cytokine activity in microglia.

To investigate this cell-type-specific molecular signature further, we assessed chromatin accessibility for activity-induced genes using single nuclear assay for transposase-accessible chromatin with sequencing (snATAC-seq)[16] on human samples from the stimulated paradigm. We found enriched promoter accessibility for 21 genes in microglia that exhibited upregulated gene expression in the bulk RNA seq and snRNAseq data (**Fig. 3a-b, Supplementary Table 5**), showing upregulation of transcription factors *FOS*, *NR4A1*, *NR4A2*, and *NR4A3* and cytokine-related genes *CCL4, CCL4L2* and *OSM.* Next, we performed transcription factor motif analysis using

the sn-ATAC seq data from microglia and found an enrichment of binding motifs for SPIC, KLF6, SPI1, HOXB13, REL, and CREB1 (**Fig. 3c**). Notably, CREB, a master regulator of activity-induced genes has been previously shown to be activated in microglia[17]. pREL/NF-kB is a critical regulator of proinflammatory gene expression[18], including genes encoding cytokines *IL1A* and *IL1B*, which were upregulated in our snRNA-seq data (**Fig. 2d**). SPI1 is a central transcription factor essential for microglia development and activation[19], and we found specific enrichment of SPI1 on the promotor region for *CCL4* only in microglia, consistent with our snRNA-seq data (**Fig. 3d**). Within neuronal populations, the promoter region for *NPAS4* exhibited increased accessibility in excitatory and inhibitory neurons in a region bound by CBP (**Fig. 3e**), a transcriptional coactivator and lysine acetyltransferase that promotes the expression of activity-induced genes[20]. Thus, our sn-ATAC-seq reveals a signature of transcription factor motifs and chromatin accessibility to regulate activity-dependent gene expression in specific cell types in response to electrical stimulation.

This work is the first to define activity-induced gene expression in the human brain, revealing that electrical stimulation induces a distinct transcriptomic and epigenomic signature in specific cell types in the human brain. Genes related to DNA-binding transcription factor activity and cytokine signaling within microglia showed the greatest induction pattern, and this was conserved across species. We observed the hypothesized induction of the “classic” activity-dependent genes in neurons, but to our surprise, our single nuclei multiomics experiments revealed pronounced microglia-specific transcriptomic activation following electrical stimulation. The key observation of

an upregulation of the microglial response to electrical activation supports a paradigm shift in interpreting the transcriptomic activation pattern following neural stimulation. Microglia are critical modulators of neuronal activity, acting to suppress excessive activity by inhibiting surrounding neurons, including excitatory neurons[21]. Researchers have correlated human brain transcriptomics with prior recorded oscillatory signatures of memory consolidation in human subjects [22,23], but this prior work did not identify changes in gene expression driven by activity and they did not observe microglial-specific changes. This identification of a microglial transcriptomic response following electrical stimulation presents an important conceptual advance in our understanding of activity-dependent gene expression in the human brain.

Our analyses identified critical molecular components that drive activity-dependent changes in the function of brain circuits. Within neuronal cell types, the highest fold change was observed for the *NPAS4*, which encodes a master transcriptional regulator of learning-induced genes and is critical for memory consolidation[24]. Within microglia, we identified the induction of cytokine-related genes including *CCL4*, which mediates intracellular chemokine signaling, altering microglial process extension and motility, influencing neuronal-microglial interactions, and shaping neuronal connectivity [21,25-27]. These mechanisms enable microglia to respond to neuronal activation and sculpt circuit function. Our study of chromatin accessibility defines a cell-type-specific signature of transcription factors driving these processes. Thus, our findings reveal distinct cell-type specific mechanisms of activity-dependent changes in brain function, laying the

184 groundwork for future studies to link human brain transcription to closed-loop stimulation
185 and natural experience.
186
187 **Acknowledgments**
188 We thank Rashmi N. Mueller who oversaw anesthesia to manage pain levels before,
189 during, and after surgical procedures, and Kyle S. Conway for helping with initial
190 pathological assessment. We thank the Iowa Institute of Human Genetics (IIHG) core for
191 RNA seq library preparation and sequencing. We thank the Neural Circuits and Behavior
192 Core at the Iowa Neuroscience Institute for the use of their facilities. We thank the Iowa
193 NeuroBank Core for tissue collection and storage.
194 **Funding:** This work was supported by grants from the National Institute of Health R01
195 MH 087463 to T.A., The Gary & LaDonna Wicklund Research Fund for Cognitive Memory
196 Disorders to T.A., and The University of Iowa Hawkeye Intellectual and Developmental
197 Disabilities Research Center (HAWK-IDDRC) P50 HD103556 to T.A., The National
198 Institute of Health K99/R00 AG068306 to S.C., The National Institute of Health R01
199 DC004290 to M.A.H., T.A. is supported by the Roy J. Carver chair of neuroscience, T.N.J
200 & C.I.P. are supported a Research Program of Excellence of the Carver Trust. T.N.J.
201 was supported by the Andrew H. Woods Professorship.
202 **Author contributions:**
203 S.C., M.A.H. and T.A. conceived the project, designed the experiments, and interpreted
204 the data and wrote the manuscript with inputs from all the authors. H.K. performed human
205 surgery, electrical stimulation, and resected the tissue. A.E.R .and C.K.K. processed with
206 IRB and MRI imaging registration. H.O, M.A.H, T.N-J, K.V.L provided advise on surgical

207 procedure and electrical stimulation. M.M.H provided pathological assessment. L.C.L.,
208 K.V.N., and B.J.P. collected the tissue and images during resection. B.J.P., S.C. and
209 L.C.L. generated the bulk RNA, single nuclei multiomics (RNA+ATAC) data. Y.V.
210 performed the bioinformatics analysis with inputs from E.B. and J.J.M. S.A.H. performed
211 the mouse surgery and electrical stimulation experiments. K.V.N, C.K.K, Z.K. Y.K, C.I.P,
212 M.H, J.J.M, E.B, U.M, and T.N.J. provided input on data analysis and interpretation. C.I.P.
213 and L.L. helped with manuscript writing. All authors discussed the results and commented
214 on the manuscript.
215
216 **Competing interests**
217 T.A. is a scientific advisor to Aditum Bio and Radius Health and he serves on the
218 scientific advisory board of Embark Neuro. T.A serves on the Scientific Advisory Board
219 of EmbarkNeuro and is a scientific advisor to Aditum Bio and Radius Health. The other
220 authors declare no conflicting interests.
221
222 **Figure legends**
223 **Figure 1**. **Stimulation alone induces gene expression changes in cytokine activity**
224 **and DNA-binding transcription factor activity**. **a,b**. Schematics of stimulated (**a**) and
225 unstimulated (**b**) paradigms in the human anterior temporal lobe. For both paradigms
226 sample A was taken at T = 0 minutes then an adjacent sample B was taken at either T =
227 30 minutes after stimulation (**a**, stimulated paradigm, n=4 subjects) or T = 30 minutes
228 after sample A was taken (**b**, unstimulated paradigm, n=4 subjects). **c.** Volcano plots
229 showing gene expression changes in the stimulated paradigm. The most significant

genes (FDR < 0.05) are labeled in red (upregulated) or in blue (downregulated). **d.** STRING network of significantly affected genes from the stimulated paradigm showing a cytokine activity network in teal and a DNA-binding transcription factor activity network in green. The gene labels are colored based on the directionality of gene expression changes (blue = downregulated, red = upregulated). **e**. Volcano plots showing gene expression changes in the unstimulated paradigm. The most significant genes (FDR < 0.05) are labeled in red (upregulated) or in blue (downregulated).

Figure 2. Cell-type specific gene expression changes following electrical stimulation in human brain. a-c. Our multiomic approach (**a**) leads to the identification of specific cell-types (**b**) validated by the expression of specific biomarkers (**c**) using the RNA part of the assay. **d**. Heat map showing cell type specific expression of genes that were found to be differentially expressed in the bulk RNA seq. The fold-change of each gene is represented from blue (down-regulated) to red (up-regulated). **e,f.** Violin plots showing gene expression changes of CCL3, CCL4, NPAS4 and EGR4 in each cell-type for baseline (blue) and stimulated (red) conditions. A gene is either significantly upregulated (FDR number in red above the plot) or not significant (N.S. above the plot). **g**. Quadrant plot comparing gene expression changes (log10(FDR)*log2fold-change) between our bulk RNA-seq experiment (x-axis) and our multiomic snRNA-seq (y-axis) after stimulation. Genes in red in the top-right corner of the plot are significantly upregulated in both experiments. FDR thresholds of 0.05 are represented by dotted lines. The dashed line represents the linear regression applied to this quadrant plot. The R-squared value and its Pearson score statistic of the linear regression is displayed in

the top right corner of the plot. The doted lines represent the FDR < 0.05 threshold. Most significant genes affected are labeled.

Figure 3. **Differential transcription start site accessibility correlates with gene expression changes after simulation**. **a**. Volcano plot showing differential transcription start site accessibility in microglia after stimulation. A gene is labeled if its gene expression and transcription start site accessibility are significantly increased after stimulation in both bulk RNA-seq and snATAC-seq respectively. **b**. Quadrant plot comparing changes (log10(FDR)*log2fold-change) between gene expression of the RNA assay (x-axis) and transcription start site accessibility (y-axis) in the microglia cluster after stimulation. Genes in red in the top-right corner of the plot are significantly upregulated in both experiments. FDR thresholds of 0.05 are represented by dotted lines. The dashed line represents the linear regression applied to this quadrant plot. The R-squared value and its Pearson score statistic of the linear regression is displayed in the top right corner of the plot. The doted lines represent the FDR < 0.05 threshold. Most significant genes affected are labeled. **c**. DNA motifs that are overrepresented in a set of peaks that are differentially accessible in microglia after stimulation. Motifs are ranked based on significance from the most significant left to right. **d-e**. Coverage plot for CCL4 **(d)** and NPAS4 **(e)** from our multiomic experiment. Each track represents normalized chromatin accessibility signal from the ATAC assay for each cell-type and each condition (baseline or stimulated). At the end of each track there is a violin plot showing gene expression changes of the gene from the RNA assay (**** = FDR < 0.0001). Chip-seq datasets of SPI1 from Human Fujioka acute myeloid leukaemia cells [28] and CBP from human macrophages [29] are represented in the bigwig track. Genome

annotation is represented under the “Genes” track with blue rectangles representing exons and an arrow showing the direction of transcription. Individual peak computed from the peak calling is represented under the “Peak” by a grey rectangle. Each peak that may regulate the gene is linked to its transcription start site by blue arcs under the “Links” track. Genomic location and scale are located at the bottom of the plot.

Materials and Methods:

Subjects: The study subjects were 8 adult neurosurgical patients (6 female, 2 male, age 19-63 years old, median age 41 years old) with medically refractory epilepsy. The patients were undergoing surgical resection of seizure foci following non-invasive video electroencephalography (EEG) or invasive iEEG monitoring. All subjects were diagnosed with intractable epilepsy. Additionally, Subject L472 had a cavernoma and Subject L475 had a dysembryoplastic neuroepithelial tumor. All subjects except #6 were non-smokers. Subjects’ age, sex, surgery, and awake or sedative information were recorded (**Extended Data Table 1)**. All subjects were native English speakers, 7 were right-handed, 1 was left-handed, and all had left language dominance as determined by Wada tests. All subjects underwent audiometric evaluation before the study, and none were found to have hearing deficits or word recognition scores deemed sufficient to affect the findings presented in this study. The vision was self-reported as normal or corrected to normal with glasses or contact lenses. As determined by standard neuropsychological assessments, cognitive function was in the average range in all subjects. Research protocols were approved by the University of Iowa Institutional Review Board (IRB 201910791, 201911084) and the National Institutes of Health, and written informed consent was obtained from all subjects.

Procedure: Surgery was performed under general anesthesia or monitored anesthetic care. Standard craniotomy was performed by the same senior epilepsy surgeon in all patients to reach the epilepsy focus, which involved the anterior and medial temporal lobe in all patients except one who had a temporal encephalocele and surrounding anterolateral temporal cortical focus. Cortical tissue from the anterior temporal lobe was sampled for analysis. The experimental condition was defined by an electrical "stimulation paradigm" and a control "no-stimulation paradigm**"**. The location of the sampled tissue is plotted on anatomic brain reconstructions **(Extended data fig 1).** All subjects underwent resection surgery for epilepsy of various etiologies **(Extended data fig 1).** There were 4 subjects (1 iEEG and 3 EEG patients) who underwent the "stimulation paradigm" and 4 subjects (2 iEEG and 2 EEG patients) who underwent the "no-stimulation paradigm" **(Extended Data Table 5)**.

In the "stimulation paradigm", a baseline sample was obtained from the anterior temporal cortex that would be included in the planned surgical resection. The area directly adjacent to where the baseline sample was collected was stimulated with direct bipolar electric stimulation (frequency 50 Hz, pulse duration of 0.2 ms, stimulation duration 2 min, voltage 10 V, a commonly used stimulation parameters for deep brain stimulation for example). The stimulated area was then sampled after a period of 30 minutes to allow for gene expression[30,31]. In the "no stimulation paradigm", no direct electric stimulation was performed and the area directly adjacent to the baseline sample was collected 30 minutes after initial baseline sampling.

After sampling they were immediately placed in a sterile container on dry ice. The average weight of the baseline sample was 88.0 ± 33.2 mg (mean, standard deviation) and the

adjacent sample was 113.4 ± 62.7 mg. After the collection of all samples in this fashion, they were weighed and transferred to a freezer at -80° C for storage until further testing.

Sample Localization to MNI space: All samples were from the same cortical region. Intraoperative photos of the sample sites were obtained during the time of surgery. Using subject matched preoperative T1 sequence MRI, the sample sites were mapped onto their anatomic brain reconstructions **(Extended data fig. 1)**. They were also mapped onto MNI space coordinates.

RNA extraction, library preparation, and sequencing: Total RNA was extracted from sampled human brains_using miRNeasy Mini Kit (Qiagen, CA, USA). The tissue samples were homogenized in QIAzol (Qiagen, CA. USA) stainless steel beads (Qiagen, CA, USA). Chloroform was then used for phase separation. RNA containing an aqueous layer was further purified using the RNeasy MinElute spin column. RNA was finally eluted in RNase-free water. RNA concentrations were estimated using a Nanodrop (Thermo Fisher Scientific, MA, USA) and Qubit (Thermo Fisher Scientific, MA, USA). RNA libraries were prepared at the Iowa Institute of Human Genetics (IIHG), Genomics Division, using the Illumina Stranded Total RNA Prep, Ligation with Ribo-Zero Plus (Illumina Inc., San Diego, CA). The KAPA Illumina Library Quantification Kit (KAPA Biosystems, Wilmington, MA) was used to measure library concentrations. Pooled libraries were sequenced on Illumina NovaSeq6000 sequencers with 150-bp paired-end chemistry (Illumina) at the Iowa Institute of Human Genetics (IIHG) core.

Bulk RNA sequencing analysis: RNA-seq data were processed with the bcbio-nextgen pipeline (https://github.com/bcbio/bcbio-nextgen, version 1.2.9). The pipeline uses STAR[32] to align reads to the hg38 genome build (GENCODE release M10, Ensembl 89

annotation) and quantifies expression at the gene level with featureCounts [33]. All further analyses were performed using R. For gene-level count data, the R package EDASeq was used to account for sequencing depth (upper quartile normalization)[34]. Latent sources of variation in expression levels were assessed and accounted for using RUVSeq (RUVs mode using all features)[35]. Appropriate choice of the RUVSeq parameter k was guided through inspection of principal components analysis (PCA) plots. Specifically, the smallest value k was chosen where PCA plots demonstrated replicate sample clustering in the first three principal components[36]. Differential expression analysis was conducted using the edgeR package[37]. Codes to reproduce the RNA-seq differential gene expression analysis are available at https://github.com/YannVRB/Human-brain-stimulation.git.

All the transcriptomics data have been deposited in NCBI's Gene Expression Omnibus and are accessible through GEO Series accession number GSE224952.

Downstream pathway analysis: Enrichment analysis of differentially expressed genes-associated pathways and molecular functions from the stimulated and unstimulated RNA-seq was performed with the Gene Ontology (GO–molecular function) databases. Only the pathways with an adjusted p-value < 0.05 were considered as significant and displayed. Data were visualized using NetworkAnalyst (www.networkanalyst.ca). The protein-protein interactive network was constructed using STRING (version 11.5), which uses the STRING database (http://string-db.org/). The PPI network was constructed to identify the interactions between proteins encoded by differentially expressed genes (FDR<0.05) based on experimental data. The differentially expressed genes names were pasted into the "STRING protein query." Active interaction sources, including text mining,

experiments, databases, coexpression, neighborhood, gene fusion, and co-occurrence, were applied, and high interaction score confidence (0.700) was selected to construct the PPI network. Full network was constructed, where the edges indicate both functional and physical protein associations. The network edges were constructed based on evidence, where line color indicates the type of interaction evidence.

Single-nuclei multiomics (nuclei isolation, library preparation, sequencing): Nuclei were isolated from brain tissue using the Chromium Nuclei Isolation Kit (10X Genomics). Briefly, frozen tissue was dissociated with pestle in lysis buffer, passed through nuclei isolation column and spun at 16,000 rcf for 20 sec at 4^0C. Flowthrough was vortexed and spun at 500 rcf for 3 mins at 4^0C. Pellet was resuspended with debris removal buffer and centrifuged at 700 rcf for 10 mins at 4^0C, nuclei resuspended in wash buffer and centrifuged again at 500 rcf for 5 mins at 4^0C. Pellet was resuspended in resuspension buffer and nuclei were counted using a hemocytometer. Nuclei were directly processed for droplet capture for single cell multiome ATAC + gene expression using a chromium controller (10X Genomics). Chromium Next GEM Single Cell Multiome ATAC + Gene v1 chemistry was used to create single nuclei ATAC and RNA libraries from the same cell. Two baseline and two stimulated samples were used for independent replicates. Libraries were sequenced on an Illumina Novaseq 6000 with a 150 bp paired end read setup.

Single-nuclei multiomic data processing and analysis:

Raw sequencing data were processed using the Cell Ranger ARC pipeline (v2.0.2) with the cellranger-arc mm10 reference. Default parameters were used to align reads, count unique fragments or transcripts, and filter high-quality nuclei. Individual HDF5 files for each sample containing RNA counts and ATAC fragments per cell barcode were loaded

into Seurat (Read10X_h5) resulting in four Seurat objects, each containing both RNA and ATAC assays. Nuclei with outliers ATAC and RNA QC metrics (<1,000 and >100,000 ATAC read counts, <1,000 and >25,000 RNA read counts, nucleosomal signal > 2, TSS enrichment < 1, and percentage of mitochondrial reads > 20) were removed. To correctly identify cell type-specific signature, the RNA assay was chosen because it leads to less background noise for the expression of biomarkers.

To analyze the RNA part of the human brain stimulation multiomic data, gene counts were normalized and log transformed (LogNormalize), and the top 2,000 most variable features between each nuclei were identified using FindVariableFeatures (selection.method = 'vst'). Features that are repeatedly variable across nuclei and datasets were selected for integration (SelectIntegrationFeatures). We then identified anchors (FindIntegrationAnchors), which took the list of 4 individual Seurat objects for each sample as input and used these anchors to integrate the four datasets together (IntegrateData). The following analyses were performed on the integrated Seurat object. Linear dimensionality reduction was performed by principal component analysis (runPCA, npcs = 25). A k-nearest-neighbors graph was constructed based on Euclidean distance in PCA space and refined (FindNeighbors, npcs = 30), then nuclei were clustered using the Louvain algorithm (FindClusters, resolution = 0.5). Clusters were visualized with UMAP (runUMAP, dims = 30). Cell types were annotated by label transfer cell labels from an existing human primary motor cortex reference dataset from the Allen Institute (doi: 10.1038/s41586-021-03465-8) (FindTransferAnchors and TransferData). Cell types identification was validated by expression of specific biomarkers (Fig. 2c). Differentially

412 expressed genes (DEGs) in individual clusters between baseline and stimulated samples
413 were calculated (FindMarkers, test.use = 'wilcox', Padj < 0.05, logfc.threshold > |0.2|).
414 To analyze ATAC part of the human brain stimulation multiomic data, prior to integrating
415 the four Seurat object, the default assay was switched to ATAC, and peak calling was
416 performed. Since the set of peaks identified by Cellranger often merges distinct peaks
417 that are close together, creating a problem for motif enrichment analysis and peak-to-
418 gene linkage, we identified a more accurate set of peaks by calling peaks using MACS2
419 (CallPeaks) on all cells together. Peaks on nonstandard chromosomes and in genomic
420 blacklist regions were removed (keepStandardChromosomes and subsetByOverlaps).
421 Normalization was performed with a frequency-inverse document frequency
422 normalization which normalizes across cells and peaks (RunTFIDF). Then, a feature
423 selection was performed using all the peaks as input (FindTopFeatures). The dimensional
424 reduction was performed on the TF-IDF normalized matrix with the selected peaks using
425 a singular value decomposition (RunSVD). To mimic the open chromatin conformation of
426 a gene, a gene activity matrix was calculated using a window of 1000bp before and after
427 the transcription start site of each protein coding gene (GeneActivity). Differentially
428 accessible transcription start sites in individual clusters between baseline and stimulated
429 samples were calculated using a logistic regression framework (FindMarkers, test.use =
430 'LR', latent.vars = 'nCount_peaks', Padj < 0.05). Motif and transcription factor enrichment
431 analysis of transcription start sites gene activity for each cluster was performed using
432 FindMotifs. The top six enriched motifs in microglia cluster are shown in **Figure. 3c**.
433 Genomic locations of typical genes like CCL4 and NPAS4 were presented (CoveragePlot)
434 and includes chip-seq datasets (bigwig) of SPI1 from Human Fujioka acute myeloid

leukaemia cells [28] and CBP from human macrophages [29]. It also includes co-accessibility between peaks and transcription start site of genes. Codes to reproduce the multiomic data analysis are available at https://github.com/YannVRB/Human-brain-stimulation.git.

Animals: Adult male C57BL/6J mice were purchased from The Jackson Laboratory were 3 to 4 months of age during experiments. All mice had free access to food and water; lights were maintained on a 12-hour light/12-hour dark cycle.

Mouse electrical stimulation: Stimulation experiments were performed in anesthetized adult male C57BL6/J mice. Anesthesia was induced with 5% isoflurane by inhalation and maintained at 1.8-2% for the duration of the experiment. The mouse was placed in a stereotax (Kopf) and a midline incision was made and the skin retracted to expose the temporal muscle bilaterally. The dorsal insertion of both temporal muscles was removed, and the muscles retracted. A 2-3 mm craniotomy was made over area AuV (centered at 2.9 mm posterior, 4.2 mm lateral, 2.8 mm ventral from Bregma based on Paxinos atlas) bilaterally to expose the cortical surface and a small square of gel foam soaked in ACSF was applied on top of the dura to prevent it from dehydrating. For each mouse the side of electrical stimulation and sham stimulation were alternated, with the sham side serving as the baseline control for gene expression profiling. Electrical stimulation was delivered through a bipolar ball electrode constructed from two silver wires in which the uninsulated tips were melted under a butane flame (1 mm tip size, 2 mm tip spacing). For both electrical and sham stimulations, the gel foam was removed and the electrode was gently lowered to make contact with the cortical surface. For electrical stimulation, a biphasic pulse train was then delivered for two minutes (8 mA, 50 Hz, 200 µs pulse width). For the sham stimulation no current was delivered but the

electrode was left in place for 2 minutes. Following electrical or sham stimulation the electrode was slowly retracted, and the exposed dura was covered with gel foam. Selection for hemisphere was performed randomly, which resulted in the order of electrical and sham stimulation alternating from mouse to mouse. No more than 5 minutes elapsed between electrical or sham stimulation of both sides. After both sides were stimulated (electrical or sham) the mouse was left in the stereotax under anesthesia for 30 minutes before euthanasia and tissue collection. Tissue samples were immediately stored at -80^{0}C in RNA later solution (Ambion).

RNA extraction, cDNA preparation and qPCRs from mouse auditory cortex: Tissue samples were homogenized in Qiazol (Qiagen) using stainless steel beads (Qiagen). Chloroform was added and centrifuged at 12,000*g* at room temperature for 15 min to separate RNA in the aqueous phase. RNA was precipitated in ethanol and cleared using RNeasy kit (Qiagen). RNA eluted in nuclease-free water was then treated with DNase (Qiagen) at room temperature for 25 min to remove genomic DNA. RNA was further precipitated in ethanol, sodium acetate (pH 5.2) and glycogen overnight at −20°C. RNA was precipitated by centrifugation at 30,000g for 20 min, precipitate washed with 70% ethanol and the dried RNA pellet was resuspended in nuclease-free water. RNA concentration was measured using NanoDrop (Thermo Fisher Scientific). 1 µg of RNA was used for complementary DNA (cDNA) preparation using the SuperScript IV First-Strand Synthesis System (Ambion). Real-time reverse transcription polymerase chain reactions (RT-PCRs) were performed on the QuantStudio 7 Flex Real-Time PCR System (Applied Biosystems, Life Technologies). Data were normalized to housekeeping genes (*Tubulin*, *Pgk1*, and *Actin*), and $2^{(-\Delta\Delta Ct)}$ method was used for gene expression analysis.

481 ***Statistics***: For the qPCR analysis, the Wilcoxon matched pairs signed rank test and one

482 sample Wilcoxon test was performed.

483

484 **References**

485 1 Yap, E. L. & Greenberg, M. E. Activity-Regulated Transcription: Bridging the Gap
486 between Neural Activity and Behavior. *Neuron* **100**, 330-348 (2018).
487 https://doi.org:10.1016/j.neuron.2018.10.013

488 2 Sagar, S. M., Sharp, F. R. & Curran, T. Expression of c-fos protein in brain:
489 metabolic mapping at the cellular level. *Science* **240**, 1328-1331 (1988).
490 https://doi.org:10.1126/science.3131879

491 3 Guzowski, J. F., McNaughton, B. L., Barnes, C. A. & Worley, P. F. Environment-
492 specific expression of the immediate-early gene Arc in hippocampal neuronal
493 ensembles. *Nat Neurosci* **2**, 1120-1124 (1999). https://doi.org:10.1038/16046

494 4 Laricchiuta, D. *et al.* Optogenetic Stimulation of Prelimbic Pyramidal Neurons
495 Maintains Fear Memories and Modulates Amygdala Pyramidal Neuron
496 Transcriptome. *Int J Mol Sci* **22** (2021). https://doi.org:10.3390/ijms22020810

497 5 Bali, P. & Kenny, P. J. Transcriptional mechanisms of drug addiction. *Dialogues*
498 *Clin Neurosci* **21**, 379-387 (2019).
499 https://doi.org:10.31887/DCNS.2019.21.4/pkenny

500 6 Fernandez-Albert, J. *et al.* Immediate and deferred epigenomic signatures of in
501 vivo neuronal activation in mouse hippocampus. *Nat Neurosci* **22**, 1718-1730
502 (2019). https://doi.org:10.1038/s41593-019-0476-2

503 7 Marco, A. *et al.* Mapping the epigenomic and transcriptomic interplay during
504 memory formation and recall in the hippocampal engram ensemble. *Nat Neurosci*
505 **23**, 1606-1617 (2020). https://doi.org:10.1038/s41593-020-00717-0

506 8 Reijmers, L. G., Perkins, B. L., Matsuo, N. & Mayford, M. Localization of a stable
507 neural correlate of associative memory. *Science* **317**, 1230-1233 (2007).
508 https://doi.org:10.1126/science.1143839

509 9 Halder, R. *et al.* DNA methylation changes in plasticity genes accompany the
510 formation and maintenance of memory. *Nat Neurosci* **19**, 102-110 (2016).
511 https://doi.org:10.1038/nn.4194

512 10 Boulting, G. L. *et al.* Activity-dependent regulome of human GABAergic neurons
513 reveals new patterns of gene regulation and neurological disease heritability. *Nat*
514 *Neurosci* **24**, 437-448 (2021). https://doi.org:10.1038/s41593-020-00786-1

515 11 Inman, C. S. *et al.* Direct electrical stimulation of the amygdala enhances
516 declarative memory in humans. *Proc Natl Acad Sci U S A* **115**, 98-103 (2018).
517 https://doi.org:10.1073/pnas.1714058114

12 Ezzyat, Y. *et al.* Closed-loop stimulation of temporal cortex rescues functional networks and improves memory. *Nat Commun* **9**, 365 (2018). https://doi.org:10.1038/s41467-017-02753-0

13 Scangos, K. W., Makhoul, G. S., Sugrue, L. P., Chang, E. F. & Krystal, A. D. State-dependent responses to intracranial brain stimulation in a patient with depression. *Nat Med* **27**, 229-231 (2021). https://doi.org:10.1038/s41591-020-01175-8

14 Brueggeman, L. *et al.* Drug repositioning in epilepsy reveals novel antiseizure candidates. *Ann Clin Transl Neurol* **6**, 295-309 (2019). https://doi.org:10.1002/acn3.703

15 Altmann, A. *et al.* A systems-level analysis highlights microglial activation as a modifying factor in common epilepsies. *Neuropathol Appl Neurobiol* **48**, e12758 (2022). https://doi.org:10.1111/nan.12758

16 Morabito, S. *et al.* Single-nucleus chromatin accessibility and transcriptomic characterization of Alzheimer's disease. *Nat Genet* **53**, 1143-1155 (2021). https://doi.org:10.1038/s41588-021-00894-z

17 Gao, Y. *et al.* Microglia CREB-Phosphorylation Mediates Amyloid-beta-Induced Neuronal Toxicity. *J Alzheimers Dis* **66**, 333-345 (2018). https://doi.org:10.3233/JAD-180286

18 Tak, P. P. & Firestein, G. S. NF-kappaB: a key role in inflammatory diseases. *J Clin Invest* **107**, 7-11 (2001). https://doi.org:10.1172/JCI11830

19 Jones, R. E., Andrews, R., Holmans, P., Hill, M. & Taylor, P. R. Modest changes in Spi1 dosage reveal the potential for altered microglial function as seen in Alzheimer's disease. *Sci Rep* **11**, 14935 (2021). https://doi.org:10.1038/s41598-021-94324-z

20 Kim, T. K. *et al.* Widespread transcription at neuronal activity-regulated enhancers. *Nature* **465**, 182-187 (2010). https://doi.org:10.1038/nature09033

21 Badimon, A. *et al.* Negative feedback control of neuronal activity by microglia. *Nature* **586**, 417-423 (2020). https://doi.org:10.1038/s41586-020-2777-8

22 Berto, S. *et al.* Gene-expression correlates of the oscillatory signatures supporting human episodic memory encoding. *Nat Neurosci* **24**, 554-564 (2021). https://doi.org:10.1038/s41593-021-00803-x

23 Berto, S., Wang, G. Z., Germi, J., Lega, B. C. & Konopka, G. Human Genomic Signatures of Brain Oscillations During Memory Encoding. *Cereb Cortex* **28**, 1733-1748 (2018). https://doi.org:10.1093/cercor/bhx083

24 Ramamoorthi, K. *et al.* Npas4 regulates a transcriptional program in CA3 required for contextual memory formation. *Science* **334**, 1669-1675 (2011). https://doi.org:10.1126/science.1208049

25 Liu, Y. U. *et al.* Neuronal network activity controls microglial process surveillance in awake mice via norepinephrine signaling. *Nat Neurosci* **22**, 1771-1781 (2019). https://doi.org:10.1038/s41593-019-0511-3

26 Stowell, R. D. *et al.* Noradrenergic signaling in the wakeful state inhibits microglial surveillance and synaptic plasticity in the mouse visual cortex. *Nat Neurosci* **22**, 1782-1792 (2019). https://doi.org:10.1038/s41593-019-0514-0

27 Cheadle, L. *et al.* Sensory Experience Engages Microglia to Shape Neural Connectivity through a Non-Phagocytic Mechanism. *Neuron* **108**, 451-468 e459 (2020). https://doi.org:10.1016/j.neuron.2020.08.002

28 Simeoni, F. *et al.* Enhancer recruitment of transcription repressors RUNX1 and TLE3 by mis-expressed FOXC1 blocks differentiation in acute myeloid leukemia. *Cell Rep* **36**, 109725 (2021). https://doi.org:10.1016/j.celrep.2021.109725

29 Kang, K. *et al.* IFN-gamma selectively suppresses a subset of TLR4-activated genes and enhancers to potentiate macrophage activation. *Nat Commun* **10**, 3320 (2019). https://doi.org:10.1038/s41467-019-11147-3

30 Hansson, A. C. & Fuxe, K. Time-course of immediate early gene expression in hippocampal subregions of adrenalectomized rats after acute corticosterone challenge. *Brain Res* **1215**, 1-10 (2008). https://doi.org:10.1016/j.brainres.2008.03.080

31 Cullinan, W. E., Herman, J. P., Battaglia, D. F., Akil, H. & Watson, S. J. Pattern and time course of immediate early gene expression in rat brain following acute stress. *Neuroscience* **64**, 477-505 (1995). https://doi.org:10.1016/0306-4522(94)00355-9

32 Dobin, A. *et al.* STAR: ultrafast universal RNA-seq aligner. *Bioinformatics* **29**, 15-21 (2013). https://doi.org:10.1093/bioinformatics/bts635

33 Liao, Y., Smyth, G. K. & Shi, W. featureCounts: an efficient general purpose program for assigning sequence reads to genomic features. *Bioinformatics* **30**, 923-930 (2014). https://doi.org:10.1093/bioinformatics/btt656

34 Risso, D., Schwartz, K., Sherlock, G. & Dudoit, S. GC-content normalization for RNA-Seq data. *BMC Bioinformatics* **12**, 480 (2011). https://doi.org:10.1186/1471-2105-12-480

35 Risso, D., Ngai, J., Speed, T. P. & Dudoit, S. Normalization of RNA-seq data using factor analysis of control genes or samples. *Nat Biotechnol* **32**, 896-902 (2014). https://doi.org:10.1038/nbt.2931

36 Peixoto, L. *et al.* How data analysis affects power, reproducibility and biological insight of RNA-seq studies in complex datasets. *Nucleic Acids Res* **43**, 7664-7674 (2015). https://doi.org:10.1093/nar/gkv736

37 Robinson, M. D., McCarthy, D. J. & Smyth, G. K. edgeR: a Bioconductor package for differential expression analysis of digital gene expression data. *Bioinformatics* **26**, 139-140 (2010). https://doi.org:10.1093/bioinformatics/btp616

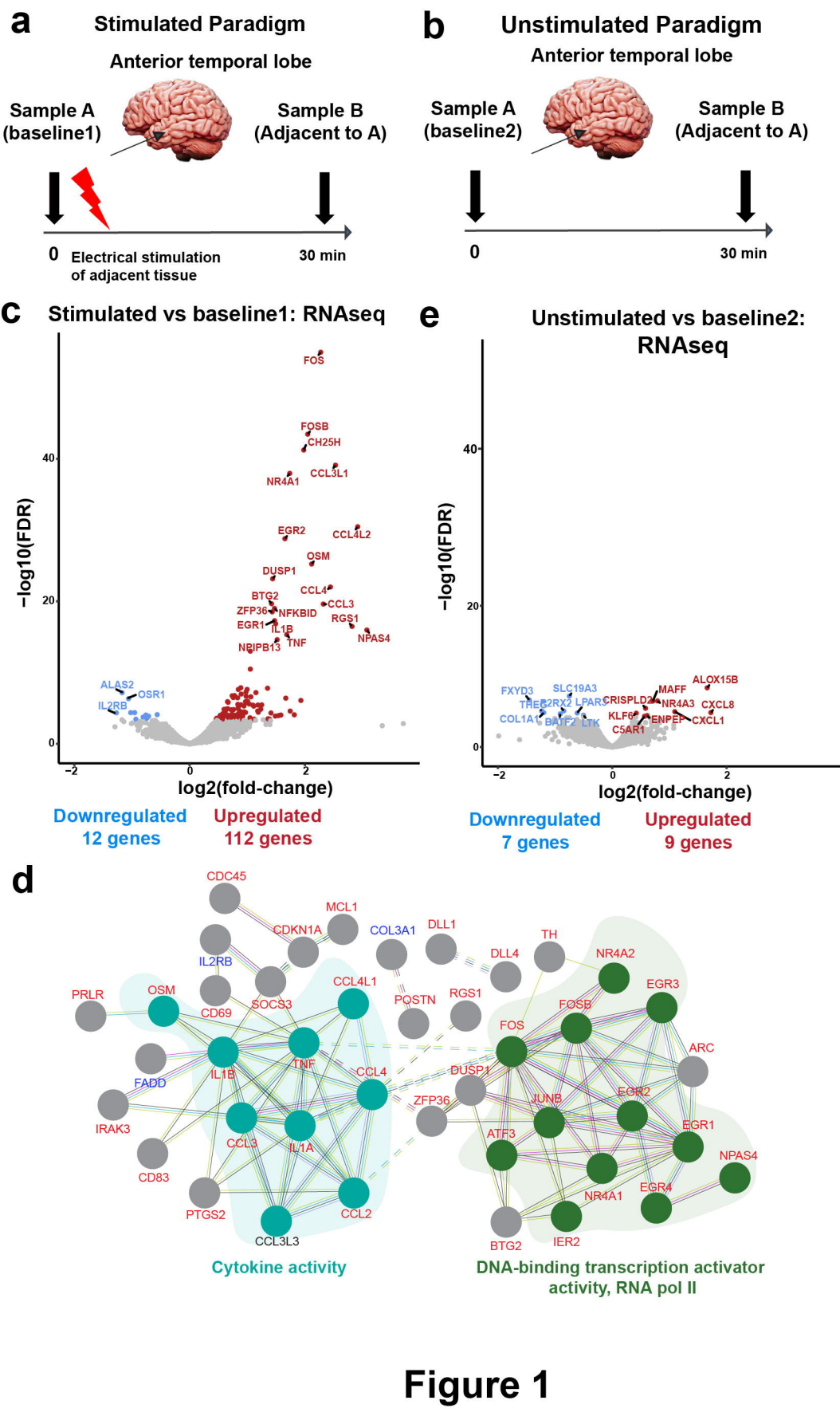
a
Stimulated Paradigm
Anterior temporal lobe
Sample A
(baseline1)
Sample B
(Adjacent to A)
0
Electrical stimulation
of adjacent tissue
30 min
b
Unstimulated Paradigm
Anterior temporal lobe
Sample A
(baseline2)
Sample B
(Adjacent to A)
0
30 min
c
Stimulated vs baseline1: RNAseq
−log10(FDR)
log2(fold-change)
FOS
FOSB
CH25H
CCL3L1
NR4A1
EGR2
CCL4L2
OSM
DUSP1
CCL4
BTG2
CCL3
ZFP36
NFKBID
RGS1
EGR1
IL1B
NPAS4
TNF
NBIPB13
ALAS2
OSR1
IL2RB
Downregulated
12 genes
Upregulated
112 genes
e
Unstimulated vs baseline2:
RNAseq
−log10(FDR)
log2(fold-change)
ALOX15B
FXYD3
SLC19A3
MAFF
CRISPLD2
NR4A3
CXCL8
THEM
S2RX2
LPAR5
KLF6
ENPEP
CXCL1
COL1A1
BATF2
LTK
C5AR1
Downregulated
7 genes
Upregulated
9 genes
d
CDC45
MCL1
CDKN1A
COL3A1
DLL1
DLL4
TH
NR4A2
EGR3
IL2RB
PRLR
OSM
CD69
SOCS3
CCL4L1
POSTN
RGS1
FOSB
FOS
ARC
TNF
IL1B
CCL4
DUSP1
FADD
ZFP36
EGR2
JUNB
IRAK3
CCL3
IL1A
ATF3
EGR1
CD83
NPAS4
EGR4
NR4A1
PTGS2
CCL2
CCL3L3
BTG2
IER2
Cytokine activity
DNA-binding transcription activator
activity, RNA pol II

Figure 1

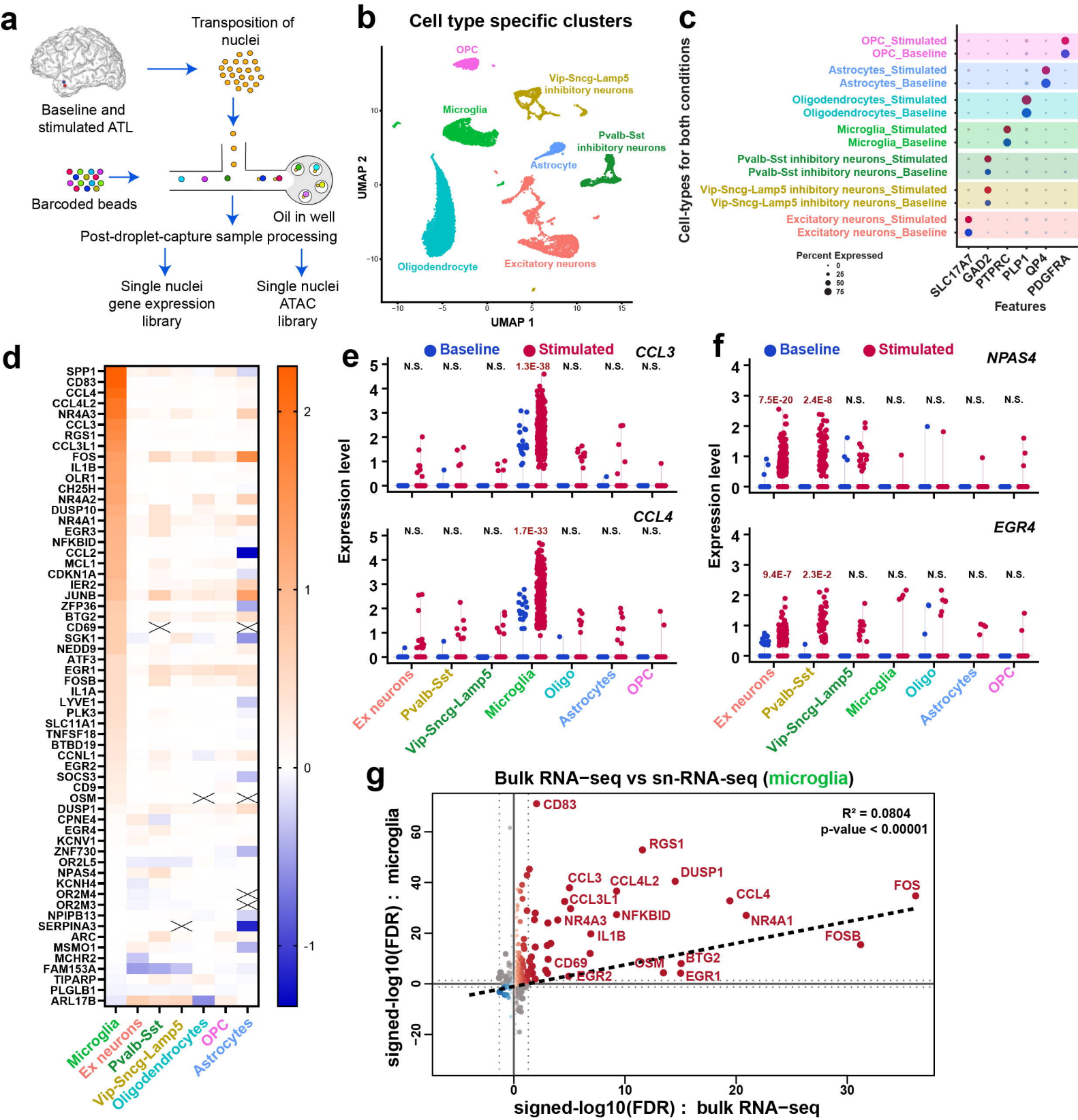
a
Transposition of nuclei
Baseline and stimulated ATL
Barcoded beads
Oil in well
Post-droplet-capture sample processing
Single nuclei gene expression library
Single nuclei ATAC library
b
Cell type specific clusters
OPC
Vip-Sncg-Lamp5 inhibitory neurons
Microglia
Pvalb-Sst inhibitory neurons
Astrocyte
Oligodendrocyte
Excitatory neurons
UMAP 2
UMAP 1
c
Cell-types for both conditions
OPC_Stimulated
OPC_Baseline
Astrocytes_Stimulated
Astrocytes_Baseline
Oligodendrocytes_Stimulated
Oligodendrocytes_Baseline
Microglia_Stimulated
Microglia_Baseline
Pvalb-Sst inhibitory neurons_Stimulated
Pvalb-Sst inhibitory neurons_Baseline
Vip-Sncg-Lamp5 inhibitory neurons_Stimulated
Vip-Sncg-Lamp5 inhibitory neurons_Baseline
Excitatory neurons_Stimulated
Excitatory neurons_Baseline
Percent Expressed
SLC17A7
GAD2
PTPRC
PLP1
QP4
PDGFRA
Features
d
SPP1
CD83
CCL4
CCL4L2
NR4A3
CCL3
RGS1
CCL3L1
FOS
IL1B
OLR1
CH25H
NR4A2
DUSP10
NR4A1
EGR3
NFKBID
CCL2
MCL1
CDKN1A
IER2
JUNB
ZFP36
BTG2
CD69
SGK1
NEDD9
ATF3
EGR1
FOSB
IL1A
LYVE1
PLK3
SLC11A1
TNFSF18
BTBD19
CCNL1
EGR2
SOCS3
CD9
OSM
DUSP1
CPNE4
EGR4
KCNV1
ZNF730
OR2L5
NPAS4
KCNH4
OR2M4
OR2M3
NPIPB13
SERPINA3
ARC
MSMO1
MCHR2
FAM153A
TIPARP
PLGLB1
ARL17B
Microglia
Ex neurons
Pvalb-Sst
Vip-Sncg-Lamp5
Oligodendrocytes
OPC
Astrocytes
e
Baseline
Stimulated
CCL3
N.S.
1.3E-38
CCL4
1.7E-33
Expression level
Ex neurons
Pvalb-Sst
Vip-Sncg-Lamp5
Microglia
Oligo
Astrocytes
OPC
f
NPAS4
7.5E-20
2.4E-8
EGR4
9.4E-7
2.3E-2
g
Bulk RNA−seq vs sn-RNA-seq (microglia)
R² = 0.0804
p-value < 0.00001
CD83
RGS1
CCL3
CCL4L2
DUSP1
CCL3L1
CCL4
FOS
NR4A3
NFKBID
NR4A1
IL1B
FOSB
CD69
OSM
BTG2
EGR2
EGR1
signed-log10(FDR) : microglia
signed-log10(FDR) : bulk RNA−seq

Figure 2

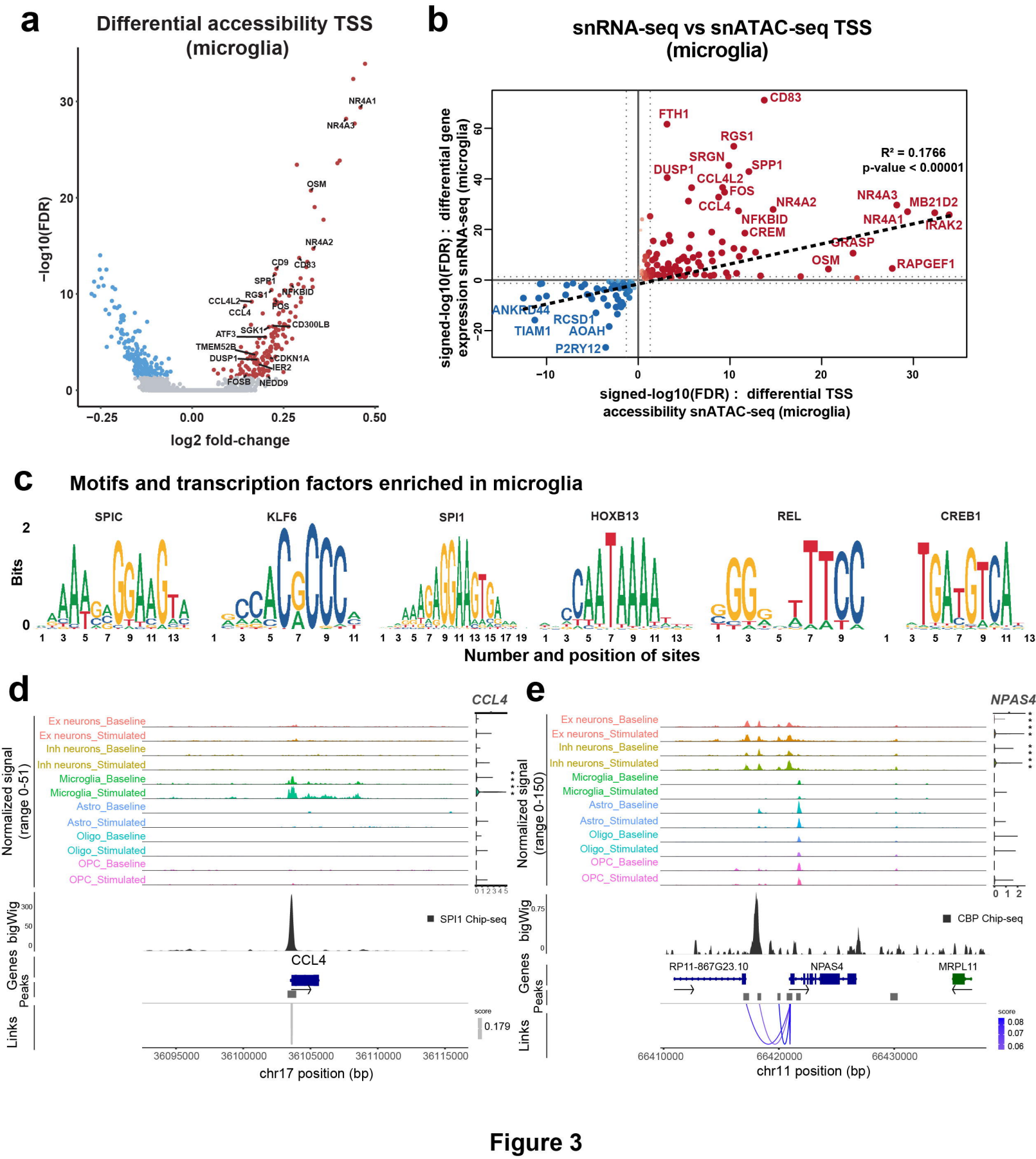
a
Differential accessibility TSS (microglia)
−log10(FDR)
log2 fold-change
NR4A1
NR4A3
OSM
NR4A2
CD9
CD83
SPP1
RGS1
NFKBID
CCL4L2
FOS
CCL4
CD300LB
ATF3
SGK1
TMEM52B
DUSP1
CDKN1A
IER2
FOSB
NEDD9
b
snRNA-seq vs snATAC-seq TSS (microglia)
signed-log10(FDR) : differential gene expression snRNA-seq (microglia)
signed-log10(FDR) : differential TSS accessibility snATAC-seq (microglia)
R² = 0.1766
p-value < 0.00001
CD83
FTH1
RGS1
SRGN
SPP1
DUSP1
CCL4L2
FOS
CCL4
NR4A2
NFKBID
CREM
NR4A3
MB21D2
NR4A1
IRAK2
GRASP
OSM
RAPGEF1
ANKRD44
RCSD1
TIAM1
AOAH
P2RY12
c
Motifs and transcription factors enriched in microglia
SPIC
KLF6
SPI1
HOXB13
REL
CREB1
Bits
Number and position of sites
d
CCL4
Normalized signal (range 0-51)
Ex neurons_Baseline
Ex neurons_Stimulated
Inh neurons_Baseline
Inh neurons_Stimulated
Microglia_Baseline
Microglia_Stimulated
Astro_Baseline
Astro_Stimulated
Oligo_Baseline
Oligo_Stimulated
OPC_Baseline
OPC_Stimulated
bigWig
SPI1 Chip-seq
Genes
CCL4
Peaks
Links
score
0.179
chr17 position (bp)
e
NPAS4
Normalized signal (range 0-150)
CBP Chip-seq
RP11-867G23.10
NPAS4
MRPL11
score
chr11 position (bp)

Figure 3